Dalton Transactions

Accepted Manuscript

ROYAL SOCIETY OF CHEMISTRY

www.rsc.org/dalton

Journal Name

ARTICLE

Novel Aminoalkyl Tris-cyclometalated Iridium Complexes as Cellular Stains

Received 00th January 20xx,
Accepted 00th January 20xx

DOI: 10.1039/x0xx00000x

www.rsc.org/

A. Sansee,[a] S. Meksawangwong,[a] K. Chainok,[b] K. J. Franz,[c] M. Gál,[d] L.–O. Pålsson,[e] W. Puniyan,[a] R. Traiphol,[f,g,h] R. Pal*,[e] and F. Kielar*[a,i]

Herein we report the synthesis and investigation of propertis of two tris-cyclometalated luminescent iridium complexes. These complexes are simple derivatives of *fac*-[Ir(ppy)$_3$] bearing amino alkyl groups on one of the phenylpridine rings. The complexes are highly emissive and exhibit structured emission peaks in aqueous solution while having only broad unstructured emission in organic solvents. The complexes have been shown to be taken up by NIH-3T3 and PC3 cells, where they localize in the lysosomes and remain emissive with lifetimes in the microsecond domain.

Dedicated to Professor David Parker FRS for the occasion of his 60th birthday

Introduction

Luminescent iridium complexes are among the new breed of luminophores receiving increasing attention due their unique and promising bio-photophysical properties.[1] Luminescent iridium complexes possess the benefits such as relatively long luminescence lifetimes and large Stokes' shifts. In addition, the photochemistry of luminescent iridium complexes is rich due to their ability to involve excited states of various characteristics (e.g. MLCT, IL, LL etc.).[1a, 2] Prototypical is the response to molecular oxygen as the excited states have a triplet character.[3] It should be noted that that luminescent iridium complexes also offer the possibility to provide lifetime based sensing as opposed to purely intensity based one. Perhaps the most interesting, among the possibilities of constructing responsive probes from luminescent iridium complexes, is the possibility to create dual emissive systems, which emit from two different excited states,[4] making it possible to create ratiometric systems.[5]

Luminescent iridium complexes distinguish themselves from other luminescent metal complexes by the possibility of facile tuning of emission wavelengths and relatively high phosphorescence quantum yields.[6]

Luminescent iridium complexes can be derived from several basic architectures. Complexes, which have received the most attention in the context of cellular imaging, are based on the bis-cyclometalated structure containing an N^N diimine ligand.[1a, 1b, 1e, 7] These complexes offer relatively straight forward synthesis and are monocationic, which helps their translocation across the cellular membrane.[1b, 1d] A number of cellular stains and responsive probes have already been developed using this type of luminescent entities.[1e, 4a, 8] Luminescent tris-cyclometalated iridium complexes constitute another common structural cast, that possess typically better photophysical properties than the bis-cyclometalated complexes mentioned above.[9] However, their use in the context of cellular imaging is rather limited in comparison to the former type. One of the reasons to this might be their limited ability to cross cellular membranes due to their lack of positive charge.[7a]

There are also several examples in the literature of tris-cyclometalated luminescent iridium complexes utilized in cellular imaging.[9-10]

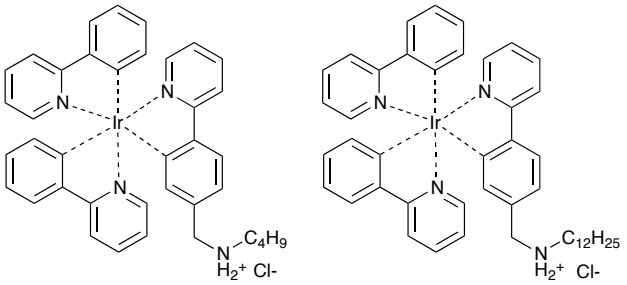

1 2

Fig. 1 Structures of iridium complexes **1** and **2**.

[a] Department of Chemistry, Naresuan University, Phitsanulok, 65000, Thailand.
[b] Department of Chemistry and Materials Technology, Thammasat University, Pathum Thani, 12130, Thailand.
[c] Department of Chemistry, Duke University, Durham, NC, 27708, USA.
[d] Department of Chemistry, Slovak Technical University, Bratislava, Slovakia.
[e] Department of Chemistry, Durham University, Durham, DH1 3LE,UK
[f] Laboratory of Advanced Polymers and Nanomaerials, Deparment of Chemistry and Center for Innovation in Chemistry, Naresuan Univesity, Phitsanulok, 65000, Thailand
[g] Program in Materials Science, Mahidol University,Faculty of Science, Bangkok, 10400, Thailand
[h] NANOTEC-MU Excellence Center on Intelligent Materials and Systems, Mahidol University, Faculty of Science, Bangkok, 10400, Thailand
[i] Center of Excellence in Biomaterials, Naresuan University, Phitsanulok, 65000, Thailand.
Email: filipkilear@nu.ac.th

† Electronic Supplementary Information (ESI) available. CCDC 1481835. For ESI and crystallographic data in CIF or other electronic format see
DOI: 10.1039/x0xx00000x

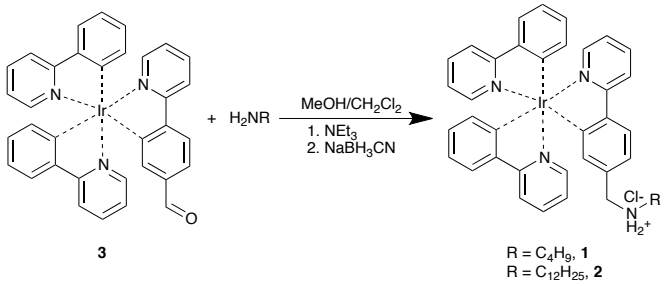

Scheme 1. Synthesis of complexes **1** and **2**.

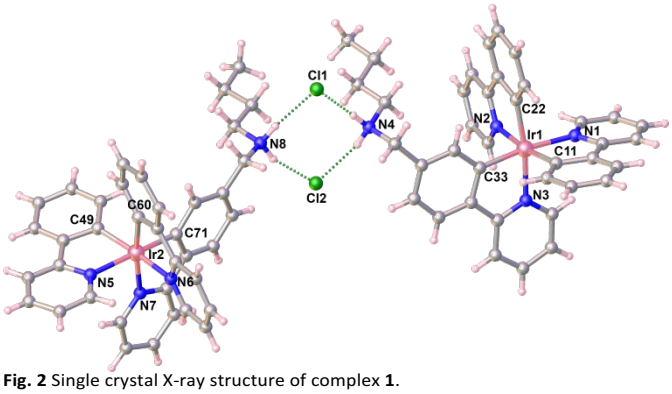

Fig. 2 Single crystal X-ray structure of complex **1**.

These indicate the necessity for the presence of a protonable group in their structure to enable them to become positively charged, which should facilitate their accumulation into cells. A recent effort in this area has been provided by the research group of Aoki, who are investigating the possibility of modifying tris-cyclometalated iridium complexes by chemical transformations and the effects these have on their behaviour in cellular systems.[8l, 11]

Luminescent iridium complexes have also been utilized in various applications as luminescent probes. Interesting recent examples of this approach have been reported by the group of Ma, who utilize G-quadruplex binding luminescent iridium complexes to detect various biologically important species.[12]

Research in our group has focused on the development of responsive luminescent iridium complexes. These have been based on both monocationic bis-cyclometalated and neutral tris-cyclometalated structures. Iridium complexes **1** and **2** (Fig.1) were synthesized both as control and precursor compounds for future responsive systems. However, their interesting luminescent properties including structured emission bands in aqueous media prompted us to investigate these complexes as potential luminescent probes for cellular imaging.

Results and discussion

Synthesis and characterization

Iridium complexes *fac*-[Ir(ppy)ppy-NC_4)].HCl (**1**) and *fac*-[Ir(ppy)ppy-NC_{12})].HCl (**2**) (ppy: 2-phenylpyridine, ppy-NC4: *N*-(4-(pyridin-2-yl)bynzyl)butan-1-amine, ppy-NC_{12}: *N*-(4-(pyridin-2-yl)bynzyl)dodecan-1-amine) have been synthesized by simple reductive ammination reaction (Scheme 1) from *fac*-[$Ir(ppy)_2$fppy] **3** (fppy: 4-(pyridine-2-yl)benzaldehyde).[13] The relative ease of both the synthesis of the precursor complex and the installation of the aminoalkyl chains suggest the possibility of using the route for the synthesis of further complex structures. The complexes were purified by column chromatography followed by their recrystallization from mixture of dichloromethane and hexane. The complexes were isolated as the hydrochloride salts and characterized by ^{1}H-, ^{13}C NMR, elemental analysis, and HRMS (ES^+). The isolation of the hydrochloride salts was not deliberate and is ascribed to the formation of HCl from impurities in the dichloromethane used in chromatographic purification.

Slow diffusion of diethyl ether into a methanolic solution of complex **1** at 4°C yielded crystals suitable for single crystal diffraction. Complex **1** crystallizes in the monoclinic space group $P2_1/c$ with two [$Ir(ppy)_2$ppy-NC_4].H^+ cations, two Cl^- anions and disordered solvent molecules in the asymmetric unit. Each Ir(III) ion is in an octahedral coordination environment formed by three nitrogen atoms and three carbon atoms from two different ppy ligands and one aminobutyl bearing ppy ligand in a *fac* configuration as shown in Fig.2. The Ir–N (2.109(4) – 2.136(4) Å) bond lengths in complex **1** are slightly longer than the Ir–C (2.003(5) – 2.017(4) Å) bond lengths and thus the [IrN_3C_3] octahedral core is slightly distorted. These structural features, however, are typical for related iridium(III) complexes containing C,N-donor set ligands.[11e] A pair of cationic [$Ir(ppy)_2$(ppy-NC_4)].H^+ complexes are linked *via* N–H···Cl hydrogen bonds between the amino groups of the ppy-NC_4 ligands and chloride anions (N4-H4···Cl1 = 3.112 (4) Å, N4-H4*B*···Cl2 = 3.077 (4) Å, N8···Cl1 = 3.139(4) Å, N8···Cl2 = 3.157(4) Å). These pairs are further linked to neighbouring pairs of molecules *via* π–π stacking interactions between the pyridine rings of the ppy-NC_4 ligands (centroid to centroid distance = 3.644(3) Å; dihedral angle = 1.25(19)°) and C–H···π interactions involving the pyridine H atom of ppy-NC_4 ligand and the benzene ring of ppy ligand (H64···centroid = 2.739(2) Å). Further details regarding this structure can be found in the electronic supplementary information.

Photophysical properties

Absorption Spectra

The absorption spectra of all three complexes, obtained in dichloromethane and shown in Fig.3, are typical for cyclometalated iridium complexes. The peaks between 250 nm and 320 nm are assigned to ligand centred π-π*transitions. The broad bands observed between 320 nm and 430 nm, on the other hand, can be assigned to spin-allowed metal to ligand charge transfer (^{1}MLCT) transitions. Finally, the tails of these bands extending beyond 500 nm, are associated with spin forbidden metal to ligand charge transfer (^{3}MLCT) transitions. These features and the slight differences between the complexes are consistent with previous reports.[13]

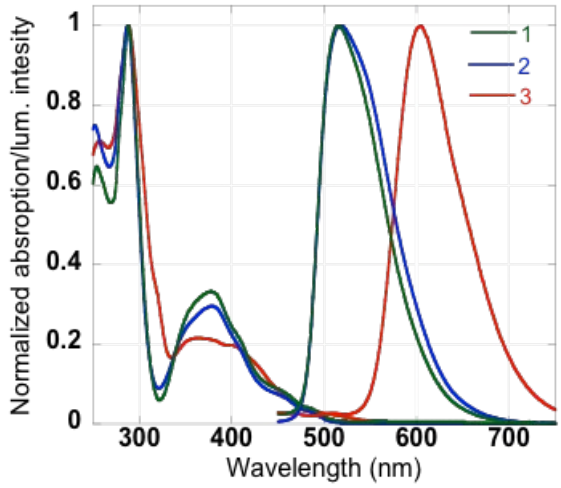

Fig. 3 Normalized absorption and emission spectra of complexes **1**, **2**, and **3** recorded in dichloromethane (10 μM). Emission spectra were recorded with λ_{ex} = 375 nm.

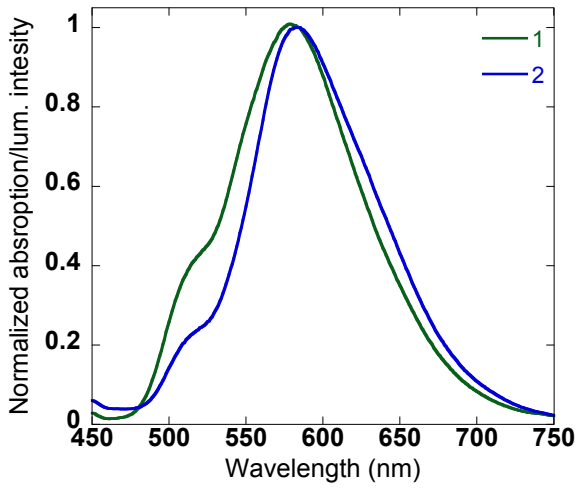

Fig. 4 Normalized emission spectra of complexes **1** and **2** (10 μM) in phosphate buffer at pH 7.5 (λ_{ex} = 375 nm).

Table 1 Photophysical properties of complexes **1**, **2**, and **3.**

	1	**2**	**3**
Absorption λ_{max}/nm	253, 288, 375	251, 287, 380	254, 288, 358, 406
Emission λ_{max}/nm	515	515	610
Emission λ_{max}/nm	510	510	573
Quantum Yield ϕ_{lum}	0.38	0.34	0.03
Emission 77 K λ_{max}/nm	501, 536	521, 548	591, 627

Steady State Emission Properties

Emission spectra of the three complexes obtained in dichloromethane are also shown in Fig. 3. The spectra exhibit broad bands typical of emission of cyclometalated iridium complexes. A significant difference in the position of the emission maxima is observed. Complexes **1** and **2** show maximum emission wavelength at 515 nm while complex **3** has its emission maximum at 610 nm. These differences have been observed before for analogous structures and the behaviour of complex **3** has previously been rationalized by the involvement of the formyl group in its excited states.[13] One of the observations made previously was the significant solvatochromism of emission of complex **3**.

Therefore, the emission spectra of the three complexes have been recorded in toluene (Figure S6). The figure shows that the emission maximum of complex **3** has shifted to 573 nm, as previously observed, while that of complexes **1** and **2** moved only to 510 nm. These differences in the photophysical behavior of the complexes are further stressed by the values of the quantum yields. Complexes **1** and **2** exhibit luminescence quantum yields, in degassed dichloromethane, in excess of 30%. On the other hand, complex **3** has a quantum yield of only 3%. Once again these values are consistent with previous observations.[13b] Essentially the photophysical behaviour of complexes **1** and **2** is very close to that of *fac*-[Ir(ppy)$_3$] indicating minimal influence of the aminoalkyl substituents. On the other hand, the formyl group in complex **3** imparts significantly different photophysical behaviour. The above results are summed up in Table 1. Interestingly, the emission spectra of complexes **1** and **2** in aqueous media (50 mM phosphate buffer, pH 7.5) are structured (Fig. 4). They contain features at both 520 and 580 nm. The emission spectrum of complex **3** in aqueous media exhibits only weak emission with maximum at 610 nm as was the case in dichloromethane. The relative intensity of the two features observed in the emission spectra of complexes **1** and **2** is dependent on structure as evidenced by the fact that the ratio is different for complex **1** and **2**. It is expected that the peak at 580 nm corresponds to an aggregated state of the complexes, while the feature at 520 nm is for a fully solvated state. This assumption is also supported by the fact that the spectral form of the complexes is concentration dependent, especially for complex **1**. Lowering the concentration to 1 μM for complex **1** leads to a significant change of the ratio of emission intensity at 520 and 580 nm, while only minimal change is observed in the spectrum of complex **2** (Fig S8). Complex **2**, containing a significantly longer alkyl chain than complex **1**, is expected to be more likely to aggregate and thus show smaller sensitivity to concentration.

Time Resolved Luminescence Measurements

Time resolved luminescence measurements were carried out with complexes **1**, **2**, and **3** to gain further understanding into their photophysical properties. The measurements were carried out in dichloromethane, tetrahydrofuran, and phosphate buffer. The decays in both organic solvents are monoexponential for all of the complexes. This is shown for air equilibrated solutions in dichloromethane in Fig. S9. The fitted lifetimes are shown in Table 2 and the values are consistent with previously reported data.[13b] As expected, the lifetimes show sensitivity to oxygen. Interestingly, this effect is much more significant for complexes **1** and **2** for which the lifetimes

Table 2 Luminescent lifetimes (μs) obtained for 10 μM solutions of complexes **1**, **2** , and **3** various media (λ_{ex} = 375 nm) (Values is brackets are for measurements in degassed solutions)

	1	**2**	**3**
Dichloromethane	0.06	0.05	0.09
	(1.56)	(1.55)	(0.25)
Tetrahydrofuran	0.03	0.04	0.07
	(1.59)	(1.59)	(0.61)
Phosphate buffer	0.10, 0.39	0.10, 0.56	-
In cellulo	0.97	1.17	-

increase from values in the range 30-60 ns, in air equilibrated solutions, to values in excess of 1.5 μs in degassed solutions.

For complex **3** the luminescence lifetime increases from 90 ns and 70 ns, in air equilibrated solutions, to 250 ns and 610 ns, in degassed solutions, in dichloromethane and tetrahydrofuran, respectively. These properties once again show that complexes **1** and **2** exhibit properties similar to *fac*-[Ir(ppy)$_3$], while complex **3** is significantly different.[13b, 14]

Time resolved measurements were also carried out for solutions of complexes **1** and **2** in phosphate buffer (50 mM, pH 7.5). The intensity decays, unlike for the solutions in the organic solvents, are multiexponential (Figure S10). For both complexes two lifetimes between 100 ns and 1 μs can be found. These results further support the idea that the photophysical properties of these complexes in aqueous media are affected by aggregation.

Theoretical Calculations

Density Functional Theory (DFT) calculations have been performed to investigate these three complexes and gain further insights into their properties. The geometry optimizations and frequency calculations were done at the B3LYP/LANL2DZ level of theory.

The calculations were performed both in vacuum and with solvation modelled using the polarisable continuum model (acetonitrile and dichloromethane). The structural parameters of the optimized structure for complex **1** correspond well with the experimental results from X-ray crystallographic data.

Images of the HOMO and LUMO orbitals for the calculation carried out in vacuum can be seen in Fig. 5. The HOMO orbitals of complexes **1** and **2** are localized on the iridium atom and the phenyl rings of the unsubsituted ppy ligand. The LUMO orbitals of these complexes are localized on the phenyl ring of the substituted ppy ligand. On the other hand, the HOMO orbital of complex **3** is localized entirely on the iridium atom. The LUMO orbital of this complex is localized on the ppy ligand containing the formyl group, including the formyl group itself. This indicates that the HOMO to LUMO transition has a significant portion of metal to ligand charge transfer (MLCT) character. Furthermore, the results for complex **3** support the important role of the formyl group in the photophysical properties of this compound.[13a]

The energies of the HOMO and LUMO orbitals obtained for all of the calculations are shown in Table 3. It can be seen that the involvement of the solvation in the model has significant impact on the absolute energy values of the orbitals for

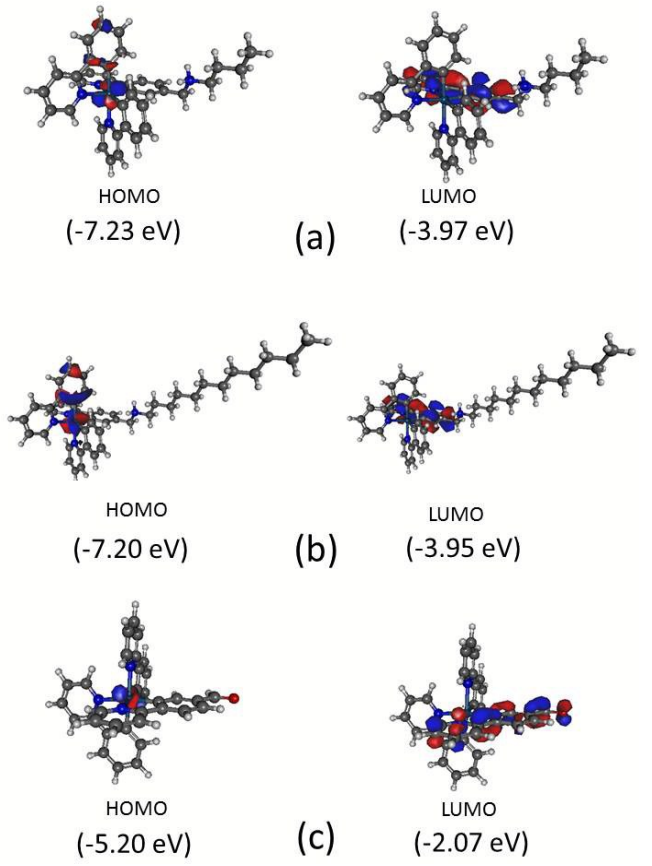

Fig. 5 The HOMO and LUMO orbitals of complexes **1** (a), **2** (b), and **3** (c) calculated in vacuum.

Table 3 Energy values of the HOMO and LUMO orbitals for complexes **1**, **2**, and **3** calculated for isolated and solvated states

		1	**2**	**3**
Vacuum	HOMO	-7.23	-7.20	-5.20
	LUMO	-3.97	-3.95	-2.07
Acetonitrile	HOMO	-5.44	-5.44	-5.41
	LUMO	-1.89	-1.89	-2.40
Dichloromethane	HOMO	-5.58	-5.58	-5.38
	LUMO	-2.06	-2.06	-2.36

complexes **1** and **2**, whereas the impact on the energy of the orbitals for complex **3** is much smaller. This is to be expected given the fact that complexes **1** and **2** are charged species while complex **3** is neutral. In all of the cases the HOMO-LUMO energy gap is bigger for complexes **1** and **2** than for complex 3. This value also changes more significantly for complexes **1** and **2** than for complex **3**. For complexes **1** and **2**, the HOMO-LUMO gap increases from less than 3.3 eV in vacuum to more than 3.5 eV in the models involving the solvents. For complex **3** the value drops from 3.13 eV in vacuum to 3.01 eV in acetonitrile and 3.02 eV in dichloromethane. The fact that the size of the HOMO-LUMO gap is at least 0.5 eV larger for complexes **1** and **2** than for complex **3** in the models including solvents indicates that a lower emission wavelength should be expected for complex **3**.

However, further calculations would be necessary to provide full explanation of the observed emission spectra.

Electrochemistry

The redox behavior of all compounds was studied by cyclic voltammetry in 0.1M $TBAPF_6$ solution in dry acetonitrile using Pt disk electrode as the working electrode (Fig. 6). All compounds are characterized by well-developed oxidation peak followed by another broad peak which is located approximately 0.5 V positively from the first peak. While the position of the first peak depends on the structure of the respective compound the position of the second peak is almost structurally independent. The height of the first peak is approximately three times higher than the height of the following one. The electrode process described by the first peak is connected with the reversible oxidation of iridium atom. The peak separation between the oxidation and the respective reduction counter peak is ca E = 80 mV for all studied compounds. The ratio between the anodic and the cathodic peak is approximately unity and the position of the peak is independent of the scan rate, which confirms the reversible behavior of the system (Fig.6, Table 3). The reaction is controlled by the diffusion, which is demonstrated by the linear dependence of the peak height, i_p on the square root of the scan rate, $v^{1/2}$. Moreover, the dependence of logarithm of anodic peak current vs. logarithm of scan rate gave a straight line with a slope of 0.48, which is close to the theoretical value of 0.5 for a purely diffusion controlled process.

Complexes **1** and **2** are oxidized at approximately the same potential 0.82 V and 0.84 V vs RE, respectively. This finding corresponds well with the theoretical calculations, where HOMO energies are almost the same for these compounds. The first oxidation potential of complex **3** appears at 0.70 V vs. RE, that means that complex **3** is oxidized more easily than the other two. The different position of the oxidation peak in the case of complex **3** is in accordance with theoretical calculations (Fig. 5). All of these values also correspond with previously reported results.[14].

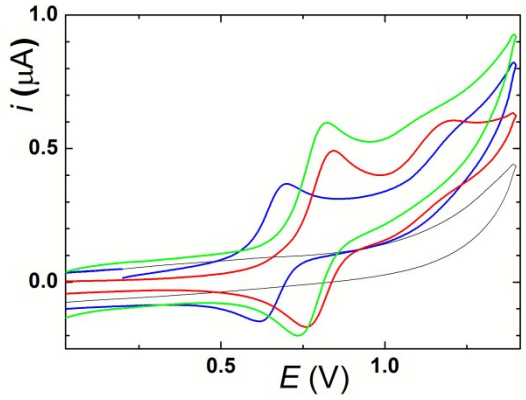

Fig. 6 Cyclic voltammograms of compound **1** (red line), **2** (green line), and **3** (blue line); background current - black line; scan rate 128 mV s^{-1}.

The following oxidation process is irreversible and is probably connected with further oxidation of respective iridium complex, which is however affected by the nature of the substituent The second oxidation peak is well pronounced for complex **1** with the shortest aliphatic chain. The second oxidation peak in the case of the complex **2** with longer aliphatic chain and complex **3** with different substituent is, however hardly visible. Also the respective reduction peak is slightly visible only in the case of complex **1** (Fig 6).

Responsive Behavior

The interesting luminescence spectral profile of complexes **1** and **2** in aqueous buffer and its concentration dependence prompted us to investigate further the aggregation of these complexes as a presumed source of this behaviour. Thus, dynamic light scattering experiments for solutions of complexes **1** and **2** (10 μM) in various mixtures of acetonitrile and water (0%, 20%, 40%, 60%, 80%, and 100% v/v of water) were performed. Corresponding emission spectra were acquired as well (Fig.7). No sign of aggregation was detected in the dynamic light scattering experiments for solutions containing 0%, 20%, and 40% v/v of water.

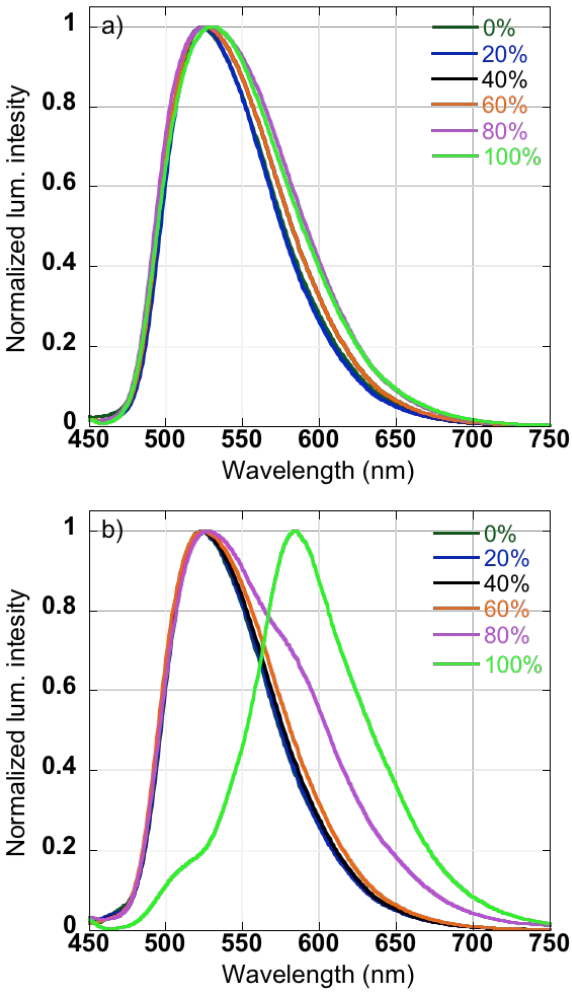

Fig.7 Normalized emission spectra of complexes **1** (a) and **2** (b) in water/acetonitrile solvent mixtures with varying amounts of water (% v/v)

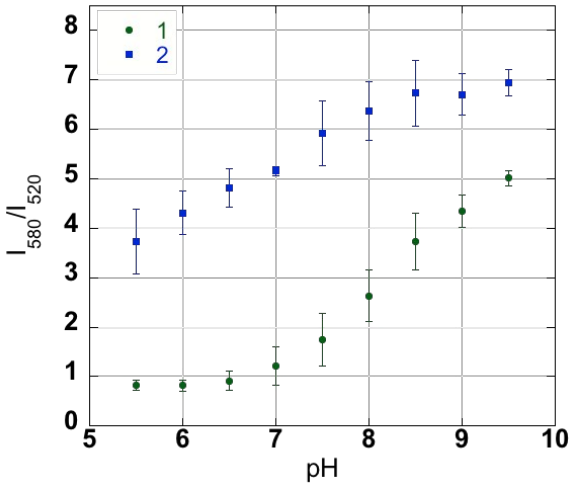

Fig. 8 Ratio of the emission intensity of complexes **1** and **2** at 580 nm and 520 nm as a function of pH.

Aggregates with size 549.5 nm (PDI: 0.388) were detected for complex **2** in the solvent mixture containing 60% v/v of water (Fig. S11). No aggregates were detected for complex **1** in this solvent mixture. However, no significant spectral changes were seen in the emission of complex **2**. Aggregates were observed for both complexes in solvent mixture containing 80% v/v of water. The sizes were 370.9 nm (PDI: 0.343) and 191.9 nm (PDI: 0.204) for complexes **1** and **2** respectively (Fig. S12). Presence of larger aggregates (> 1 μm) was detected for complex **2**. There were no changes in the emission spectra for complex **1** but a feature at 580 nm appeared in the emission of complex **2** (Fig. 7). Finally, in pure water complex **1** shows aggregates with the size of 573.7 nm (PDI: 0.772). Presence of large species (> 1 μm) can be seen in this case (Fig. S13). The dynamic light scattering experiment was not successful for complex **2** in pure water most likely due to presence of very large aggregates. The feature at 580 nm became dominant in the emission spectrum of complex **2**, while there were no significant changes in the emission spectrum of complex **1** (Fig. 7). In summary, these experiments indicate a complicated aggregation behaviour in the solutions of complexes **1** and **2**, with the possibility of formation of various types of aggregated species depending on the specific conditions. Furthermore, the original assumption that the features in the emission spectra at 520 and 580 nm can be assigned to fully solvated and aggregated species, respectively, has been shown to be wrong. The results instead indicate that the appearance of the band centred at 580 nm arises from changes in the aggregates.

Based on the previous results, we decided to investigate the response of the emission spectra of complexes **1** and **2** to pH. pH was selected to be the investigated property as the protonation and deprotonation of the amino group, which will result in the change of the charge carried by the complex, should alter the propensity to aggregate of these molecules. Indeed, a change in the ratio of emission intensity at 580 and 520 nm was observed for both complexes **1** and **2**. However, more significant and abrupt change in the ratio was observed for complex **1** (Fig. 8), changing from a value of 0.8 at pH 5.5 to 5.0 at pH 9.5. In the case of complex **2**, the ratio changes from a value of 3.7 at pH 5.5 to a value of 6.9 at pH 9.5. The shapes of the curves are also different. Complex **1** limited change in the ratio below pH 7.0 and a linear increase after that, whereas the trend for complex **2** is linear from pH 5.5 to pH 8.5 followed by a plateau. The slopes for the linear parts of the graphs for complex **1** and complex **2** are 1.7 and 1.1, respectively, indicating the more rapid change for complex **1**. This behaviour can again be rationalized by a higher propensity of complex **2** to aggregate, which is altered only to a limited extent even after the protonation of the amino group. On the other hand, the ability to aggregate is much more sensitive to protonation in the case of the less lipophilic complex **1.** It should be noted that the change in the emission properties of complex **1** in response to pH is observable by naked eye and is reversible (Figure S14). Even though a ratiometric response is observed the position of the change for complex **1** is at too high pH for biological applications. Furthermore, the dependence of the ratio on concentration and other parameters is a further complication for imaging applications.

Cellular Imaging

The encouraging photophysical properties of complexes **1** and **2** have prompted us to investigate them as potential cellular probes. This investigation was carried out using mouse skin fibroblast NIH-3T3 cell line. Cytotoxicity of the complexes was evaluated using imago-cytometry. This has shown that the IC_{50} for 24 h exposure was on the order of 5 μM with complex **1** being more toxic than complex **2** (Fig S15).

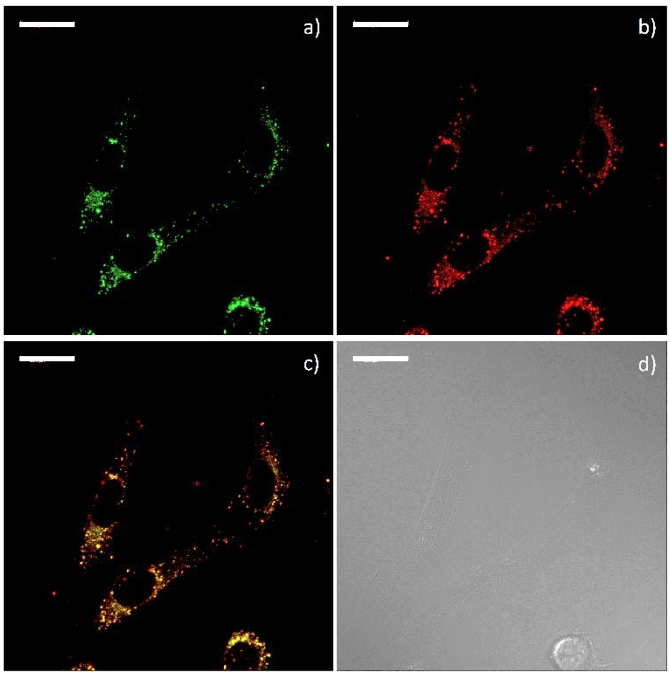

Fig. 9 Fluorescence microscopy images of NIH-3T3 cells obtained with complex **1** (λ_{ex} 355 nm, λ_{em} 450-650nm) (a), lysotracker red (λ_{ex} 543 nm HeNe laser, λ_{em} 600-650 nm), (b). Panel c shows the RGB overlay of panels a and b; P = 0.84, while panel d is the brightfield image. (Scale bar: 20 μm)

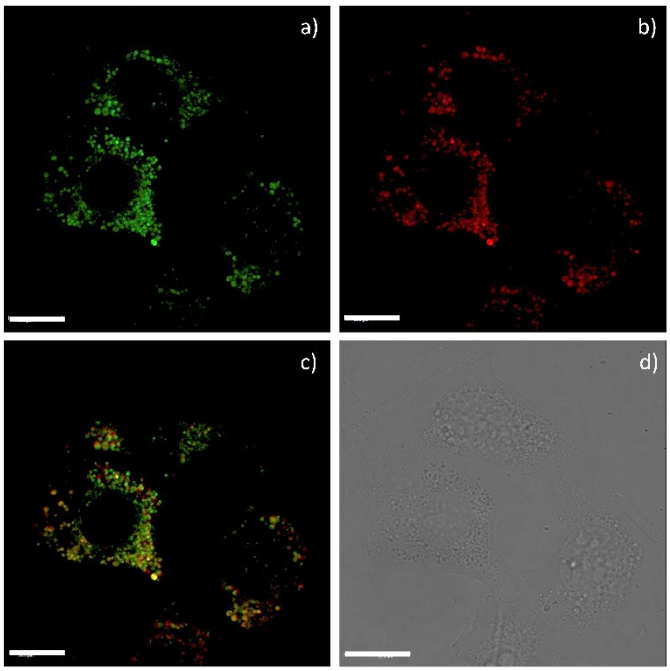

Fig. 10 Fluorescence microscopy images of NIH-3T3 cells obtained with complex **2** (λ_{ex} 355 nm, λ_{em} 450-650nm) (a), lysotracker red (λ_{ex} 543 nm HeNe laser, λ_{em} 600-650 nm) (b). Panel c shows the RGB overlay of panels a and b; P= 0.79, while panel d is the brightfield image. (Scale bar: 20 μm)

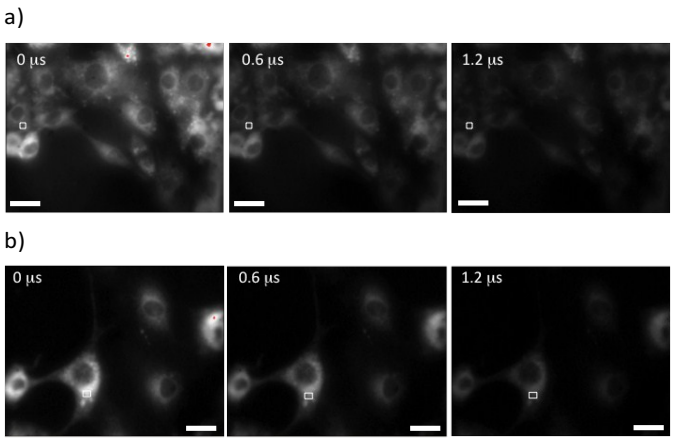

Fig. 11 Sequential time gated images for complexex **1** (a) and **2** (b) in NIH-3T3 cells at various time delays. The rectangular are is the region of interest (ROI), which was used to measure the decay of the luminescence. (Scale bar: 20 μm)

Lower cytotoxicity, especially for complex **2**, was observed after 1h incubation (Fig. S16). These results indicated the existence of a safe imaging concentration window for the two complexes as images could be acquired after shorter loading times at lower concentrations.

Complexes **1** and **2** have exhibited the ability to cross the cellular membrane and remain emissive inside the cells (Figs. 9 and 10). Images could be recorded after 30 minute incubation period (1 μM concentration). Furthermore, sufficiently bright images were obtained with loading concentration as low as 100 nM, albeit requiring a longer loading time. Loading the cells with 1 μM concentration of the complex for 1 h was used as standard procedure in the following experiments.

The emission of the complexes in the cells originated from bright spots distributed throughout the cytosol suggesting lysosomal localization. This was confirmed via co-localization experiments with LysoTracker red (Figs. 9 and 10).

It was also observed that under identical conditions complex **1** gave significantly brighter images than complex **2**. It should be noted that complex **3** gave only very faint images indicating its inability to efficiently penetrate the cellular membrane (Fig S17). Furthermore, emission spectra obtained from the cell lysates of cells treated with complexes **1** and **2** exhibited the expected emission bands for these compounds (Fig S18). Finally, the ability of complex **2** to stain NIH-3T3 cells was maintained even when the loading was performed at 4°C (Fig. S19), showing that the cellular uptake does not depend on endocytosis and is probably driven by concentration gradient dependent diffusion of the relatively lipophilic complexes. ICP-MS experiments performed with complex **2** indicated that the intracellular concentration reached 60% (±2%) of the loading concentration.

It should be noted that the imaging experiments were carried out with excitation at 355 nm (NgYAG), which is not ideal. An experiment using excitation lines at 405, 456 and even 488 nm was therefore also performed and indicated the ability to use these more favored live cell imaging excitation wavelengths to obtain images with these complexes (Fig. S20).

To further demonstrate the capabilities of these complexes, imaging experiments were performed with human prostatic adenocarcinoma, PC3, cell line using complex **2**. Images with similar localization pattern were obtained indicating the ability of these luminescent iridium complexes to act as live lysosomal stains in different cell lines (Fig. S21) without perturbing natural cell homeostasis.

The potential of complex **2** for monitoring morphological changes of lysosomes was demonstrated in respective live cell imaging experiments using both nigericin and chloroquin to achieve lysosomal pH of 5.5 (Fig. S22) and 6.6 (Fig. S23), respectively. Lysosomal swelling is observed at increasingly higher pH value and can be visualized using complex **2** (Fig. S24).

The relatively long lifetimes of luminescent iridium complexes are often quoted as a beneficial property for cellular imaging allowing the use of time resolved methods. However, this capability is rarely demonstrated or used in published studies utilizing these luminophores.[8f] We have, therefore, performed time resolved live-cell imaging experiments using complexes **1** and **2**. These experiments have shown that both complexes possess lifetimes in the microsecond range inside cells (Fig. 11). The intensity decays for the indicated regions of interest can be seen in Fig. S24 and Fig. S25. In cell luminescence lifetimes of 0.97 and 1.17 μs have been calculated based on these decays for complexes **1** and **2**, respectively. These lifetimes exceed those observed in aerated aqueous solutions but are in the range observed for degassed solutions in organic solvents (Table 2). This is likely a result of partial protection from quenching by molecular oxygen inside the lysosomes due to possible insertion of the complexes into polar binding pockets of endogenous intracellular proteins.

Conclusions

In summary we present the synthesis and characterization of two simple derivatives of $Ir(ppy)_3$. These exhibit bright luminescence with long lifetimes even in aerated aqueous solutions. Furthermore, the complexes have been shown to enter cells resulting lysosomal localization. The beneficial properties of these complexes indicate the possibility to develop more complex imaging probes based on their core structure.

Experimental

General comments

Unless otherwise stated, all commercial reagents were used as received. Silver trifluoromethanesulfonate, N-tetrabutylammonium hexafluorophosphate ($TBAPF_6$), and sodium borohydride were purhased from Sigma Aldrich. Sodium cyanoborohydride, 2-phenylpyridine (ppy), 2-ethoxyethanol, and silicagel were purchased from Merck. Butylamine, dodecylamine, 4-(2-pyridyl)benzaldehyde, and iridium(III)chloride trihydrate were purchased from Fisher. Dichloromethane, methanol, and triethyl amine were purchased from Carlo Erba. Sodium bicarbonate, sodium sulphate anhydrous, and trisodium phosphate were purchased from Univar. Acetonitrile and dimethyl sulfoxide were purchased from RCI. ^{1}H-NMR spectra were recorded on a Bruker Avance 400 MHz instrument operating at 400 MHz. Mass spectra were acquired with an Agilent technologies UHD Accurate-Mass Q-TOF LC-MS instrument model 6540. UV-Visible absorption spectra were recorded using Analytik Jena 210plus diode array spectrophotometer. Steady state emission spectra were recorded using Fluoromax-4 and Fluorolog spectrofluorometers from Yvon Horiba. Phosphorescence lifetime measurements were performed on the DeltaFlex™ instrument equipped with a UV LED (λ_{ex} = 372 nm). Dynamic light scattering was performed using Malvern Zetasizer Nano-ZS. Cell viability was determined using the Chemometec NucleoCounter cell analyzer. All of the molecular dynamics calculations were performeed using Gaussian09 program package and the molecular orbitals were visualized using the Gabedit program package.

Synthesis of aminoalkyl iridium complexes

fac-$[Ir(ppy)_2fppy]$[13a] (50 mg, 72 µmol), alkyl amine (110 µmol), and triethyl amine (10 µl, 72 µmol) were suspended in a methanol-dichloromethane (1:1) mixture (6 mL). The reaction mixture was heated to reflux for 10h. The reaction mixture was allowed to cool down and sodium cyanoborohydride (9 mg, 150 µmol) was added. The reaction mixture was stirred at room temperature for 20h. The solvent was removed under reduced pressure and the residue was dissolved in dichloromethane (20 mL). The dichloromethane solution was washed with water (2 x 15 mL), dried over sodium sulphate, filtered, and evaporated to dryness. The residue was purified by column chromatography on silica using dichloromethane with a gradient of methanol (up to 10%) as eluent. Column chromatography was followed by recrystallization from dichloromethane and hexane. The complexes were obtained as yellow-orange solids; 41 mg (53 µmol, 74%) for compex **1** and 56 mg (63 µmol, 88%) for complex **2**.

fac-$[Ir(ppy)_2(ppy\text{-}NC_4)]$.HCl (**1**)
^{1}H NMR (400 MHz, DMSO-d_6, δ) 8.73 (s, 2H), 8.20 (d, *J* = 8.0 Hz, 1H), 8.14 (d, *J* = 8.0 Hz, 2H), 7.87 (d, *J* = 8.0 Hz, 1H), 7.83-7.75 (m, 5H), 7.49 (d, *J* = 5.2 Hz, 1H), 7.45 (t, *J* = 6.0 Hz, 2H), 7.18 (d, *J* = 6.8 Hz, 1 H), 7.15-7.10 (m, 2H), 7.05 (d, *J* = 8.4 Hz, 1H), 6.85-6.79 (m, 2H), 6.73-6.61 (m, 5H), 3.74 (s, 2H), 2.68-2.64 (m, 2H), 1.48 (q, *J* = 7.2 Hz, 2H), 1.25-1.21 (m, 2H), 0.84 (t, *J* = 7.2 Hz, 3H). ^{13}C (100 MHz, DMSO–d_6, δ) 165.5, 165.5, 164.8, 161.4, 160.1, 160.0, 146.9, 146.8, 146.7, 144.8, 143.7, 137.6, 137.0, 136.2, 131.7, 129.2, 129.0, 124.3, 124.2, 123.2, 122.8, 120.7, 119.8, 119.7, 119.4, 119.1, 115.6, 114.4, 50.2, 45.6, 27.0, 19.3, 13.4. HRMS (ES^+) calcd. for $C_{38}H_{36}IrN_4$ (741.2569); found 741.2558 $[M+H]^+$. Anal. Calcd. for $C_{38}H_{36}ClIrN_4.2H_2O$: C, 56.18; H, 4.96; N, 6.90. Found: C, 56.42; H, 4.57; N, 6.74.

fac-$[Ir(ppy)_2(ppy\text{-}NC_{12})]$.HCl (**2**)
^{1}H NMR (400 MHz, $CDCl_3$, δ) 9.35 (s, 1H), 9.25 (s, 1H), 7.87 (d, *J* = 8.4 Hz, 1H), 7.84 (d, *J* = 8.4 Hz, 2H), 7.70-7.61 (m,3H), 7.60-7.52 (m, 5H), 7.48 (d, *J* = 5.2 Hz, 1H), 7.25 (m,1H), 6.91-6.76 (m, 7H), 7.00 (d, *J* = 5.2 Hz, 1H), 6.62 (d, *J* = 5.2 Hz, 1H), 6.53 (s, 1H), 3.79 (m, 2H), 2.42-2.54 (m, 2H), 1.64 (m, 2H), 1.32-1.21 (m, 18H), 0.87 (t, *J* = 6.8 Hz, 3H). ^{13}C (100 MHz, $CDCl_3$, δ) 166.7, 166.7, 165.9, 161.8, 160.8, 160.6, 147.3, 147.2, 145.1, 143.8, 143.7, 139.2, 137.0, 137.0, 136.3, 136.2, 136.2, 130.7, 130.2, 130.0, 125.0, 124.1, 122.6, 122.4, 122.2, 122.1, 121.7, 120.4, 120.1, 119.3, 119.0, 118.8, 50.3, 44.9, 32.1, 29.8, 29.7, 29.5, 29.2, 27.1, 25.8, 22.8, 14.2. HRMS (ES^+) calcd. for $C_{46}H_{52}IrN_4$ (853.3821); found 853.3836 $[M+H]^+$. Anal. Calcd. for $C_{46}H_{52}ClIrN_4.H_2O$: C, 60.94; H, 6.00; N, 6.18. Found: C, 61.31; H, 5.73; N, 6.24.

X-ray crystallography

A light yellow block-shaped crystal of ccomplex **1** with dimensions 0.26 × 0.14 × 0.12 mm was mounted on a top of fiber glass. X-ray diffraction data were collected using a Bruker D8 QUEST CMOS operating at *T* = 296(2) K. Data were measured using ω and ϕ scans of 0.5 (d, scan_width)° per frame for 30 (d, scan_rate) second using MoKα radiation (50 kV, 30 mA). The total number of runs and images was based on the strategy calculation from the program APEX2. The maximum resolution achieved was θ = 25.825°.

Unit cell indexing was refined using SAINT (Bruker, V8.34A, 2013) on 9714 reflections, 7 percent of the observed reflections. Data reduction, scaling and absorption corrections were performed using SAINT (Bruker, V8.34A, 2013) and SADABS-2014/4 (Bruker, 2014/4) was used for absorption correction.[15] wR_2(int) was 0.0857 before and 0.0616 after correction. The ratio of minimum to maximum transmission is 0.8303.The λ/2 correction factor is 0.00150. The software also corrects for Lorentz polarization. The final completeness is

99.80 out to 25.825 in θ. The absorption coefficient μ of this material is 3.683 at this wavelength (λ = 0.71073) and the minimum and maximum transmissions are 0.6188 and 0.7453.

The structure was solved in the space group *P*1 with the ShelXT structure solution program using combined Patterson and dual-space recycling methods.[16] The space group $P2_1/c$ (# 14) was determined by ShelXT structure solution program.[16] The crystal structure was refined by Least Squares using version 2014/7 of ShelXL. All non-hydrogen atoms were refined anisotropically. Hydrogen atom positions were calculated geometrically and refined using the riding model.

The solvent masking routine smtbx.mask was used and found four solvent-accessible voids in the unit cell.[17] Two of them are 524 A^3 in volume and contain an estimated 91 electrons; the other two are 265 $Å^3$ in volume and contain an estimated 45 electrons. These electrons are attributable to six molecules of deuterated methanol and three molecules of water, which means that there are two molecules of methanol and one molecule of water per formula unit present in this structure. The value of Z' is 2. This means that there are two independent molecules in the asymmetric unit.

Photochemical measurements

Unless otherwise stated, stock solutions of iridium complexes (0.5 mM) were prepared in DMSO. They were then diluted to their desired concentration (usually 10 μM) with the appropriate solvent. The measurements were performed in quarts cuvettes of 1 cm path length. Bubbling nitrogen gas through them for 10 minutes was used to degas solutions for lifetime measurements in the absence of oxygen.

Luminescence quantum yields were determined using *fac*-$[Ir(ppy)_3]$ in degassed dichloromethane solution as the standard, for which Φ_{lun} = 0.40. The solutions for this measurement were degassed by four cycles of freeze-pump-thaw.

Luminescence lifetimes of the complexes were measured by time-correlated-single-photon-counting (TCSPC) using a laser diode (372 nm) as the excitation source. The estimated error in the lifetimes is 10%.[8f]

DFT calculations

Calculations were carried out with the Gaussian09 software at the DFT level, using the hybrid functional B3LYP.[18] The double-zeta basis set LANL2DZ was used. The calculations were carried out for vacuum as well as acetonitrile (ε = 35.688) and dichloromethane (ε = 8.93) using the polarizible continuum model. The molecular orbitals were visualized using the Gabeit program package.[19]

Electrochemistry

n-Tetrabutylammonium and acetonitrile were supplied by Sigma–Aldrich. The indifferent electrolyte $TBAPF_6$ was dried under vacuum. Acetonitrile was dried over activated molecular sieves. Electrochemical measurements were performed using AUTOLAB instrument PGSTAT 302N (Metrohm). Electrochemical data from cyclic voltammetry were analyzed using AUTOLAB software. A three-electrode electrochemical cell was used. The reference electrode (RE), Ag|AgCl|1 M LiCl, was separated from the test solution by a salt bridge. The working electrode (WE) was Pt disk (d=0.8 mm). The auxiliary electrode was platinum net. The scan rate for the cyclic voltammetry was in the range 32-512 mV s^{-1}. Oxygen was removed from the solution by passing a stream of argon saturated with vapors of the solvent.

Dynamic Light Scattering

Solutions of complexes **1** and **2** (10 μM) were prepared in mixtures of water and acetonitrile of various compositions: 0%, 20%, 40%, 60%, 80%, and 100% v/v of water. The solvents were filtered using a 0.2 μm filter before the preparation of the solutions. The experiments and the analyses of the results was performed using Malvern software. The results are quoted as z-average obtained from the intensity plot. pH of the solutions in neat water was determined to be 7.0.

Cell Culture

A detailed investigation of the cellular behaviour of each complex was conducted using mouse skin fibroblasts (NIH-3T3) and human prostate adenocarcinoma (PC3) cell lines using fluorescence and laser scanning confocal microscopy. Cells were maintained in exponential growth as monolayers in F-12/DMEM (Dulbecco's Modified Eagle Medium) 1:1 that was supplemented with 10% foetal bovine serum (FBS). Cells were grown in 75 cm^2 plastic culture flasks, with no prior surface treatment. Cultures were incubated at 37 °C, 20% average humidity and 5% (v/v) CO_2. Cells were harvested by treatment with 0.25% (v/v) trypsin solution for 5 min at 37 ºC. Cell suspensions were pelleted by centrifugation at 1000 rpm for 3 min, and were re-suspended by repeated aspiration with a sterile plastic pipette. Microscopy Cells were seeded in 12-well plates on 13mm 0.17mm thick standard glass cover-slips or un-treated iBibi 100 uL live cell channels and allowed to grow to 40% – 60% confluence, at 37 ºC in 5% CO_2. At this stage, the medium was replaced and cells were treated with complexes and co-ctains as appropriate. For imaging DMEM media (10% FBS) lacking phenol red was used from this point onwards. Following incubation, the cover-slips were washed with phosphate-buffered saline (PBS; pH 7.4), mounted on slides and the edges sealed with colourless, quick-dry nail varnish to prevent drying out of the sample.

Cell toxicity measurements were run using a ChemoMetec A/S NucleoCounter3000-Flexicyte instrument with Via1-cassette cell viability cartridge (using the cell stain Acridine Orange for cell detection, and the nucleic acid stain DAPI for detecting non-viable cells). The experiments were done in triplicate. In cellular uptake studies Cells were seeded in 6-well plates and allowed to grow to 80% – 100% confluence, at 37 ºC in 5% CO_2. At this stage, the medium was replaced with media containing targeted complexes as detailed above and total cellular Iridium was determined using ICP-MS, inductively

coupled plasma mass spectrometry by Dr. C. Ottley in the Department of Earth Sciences at Durham University.

Steady state fluorescence microscopy

Steady state fluorescence images were recorded using a PhMoNa[20] enhanced Leica SP5 II LSCM confocal microscope equipped with a HCX PL APO 63x/1.40 NA LambdaBlue Oil immersion objective. Data were collected using 5x digital magnification at 400 Hz/line scan speed (4 line average, bidirectional scanning) at 355 nm (3rd harmonic NdYAG laser) with 3 mW laser power (80 nJ/voxel). In order to achieve excitation with maximal probe emission, the microscope was equipped with a triple channel imaging detector, comprising two conventional PMT systems and a HyD hybrid avalanche photodiode detector. The latter part of the detection system, when operated in the BrightRed mode, is capable of improving imaging sensitivity by 25%, reducing signal to noise by a factor of 5. Frame size was determined at 2048 x 2048 pixel, with 0.6 airy disc unit determining the applied pinhole diameter rendering on voxel to be corresponding to 24.02 x 24.02 nm (frame size 49.16 x 49.16 µm) with a section thickness of 380 nm. A HeNe or Ar ion laser was used when commercially available organelle-specific stains (e.g. LysoTrackerRed™) were used to corroborate cellular compartmentalization. Spectral imaging on this Leica system is possible with the *xyλ*-scan function, using the smallest allowed spectral band-pass (5nm) and step-size (3nm) settings. However, much improved spectral imaging in cells was achieved using a custom built microscope (modified Zeiss Axiovert 200M), using a Zeiss APOCHROMAT 63x/1.40 NA objective combined with a low voltage 365 nm pulsed UV LED focused, collimated excitation source (1.2W). For rapid spectral acquisition the microscope was equipped at the X1 port with a Peltier cooled 2D-CCD detector (Ocean Optics) used in an inverse 100 Hz time gated sequence. The spectrum was recorded from 400-800 nm with a resolution of 0.24 nm and the final spectrum was acquired using an averaged 10,000 scan duty cycle. Probe lifetimes were measured on the same microscope platform using a novel cooled PMT detector (Hamamatsu H7155) interchangeable on the X1 port, with the application of pre-selected interference filters matched to as selected in live cell LSCM experiments. Both the control and detection algorithm were written in LabView2011, where probe lifetime was determined by using a single exponential fitting algorithm to the monitored signal intensity decay.[21]

Time resolved luminescence imaging

Time-resolved luminescence microscopy was performed by excitation at 355 nm with the third harmonic of a Q-switched Nd:YAG laser (L4Light UVFQ-100-1-Y-355) producing optical pulses with a temporal width ~4 ns (FWHM) at 2 kHz. The microscope was a Leica 135 Axiovert epifluorescence microscope, in which the laser light was fed in through a beam expander and focused onto the sample using long working-distance objective lenses (100 x, Zeiss LD PlanNeofluar). The photoluminescence signal was detected, after passage through a corresponding dichroic mirror and 515 nm long-pass filter, using a time-gated CCD camera (Photonic Research Systems Ltd Imagex Nano CCD) with a resolution of 752 × 582 pixels. In the excitation–detection sequence, the CCD camera control unit was used to trigger the Q-switch of the laser system with a TTL pulse. The luminescence decays were recorded inselected regions of interest (ROIs) using a constant acquisition time gate with 16 different, well charactherised delay times between excitation and detection pulses.

Acknowledgements

The authors gratefully acknowledge the support of the Thailand Research Fund (RDG5680002). Furthermore, the authors also acknowledge National e-Science Infrastructure Consortium and The Royal Society URF and IES for providing financial and computing resources that have contributed to the research results reported within this paper.

References

1. Y. You, *Current opinion in chemical biology*, 2013, **17**, 699-707; M. P. Coogan and V. Fernandez-Moreira, *Chem Commun (Camb)*, 2014, **50**, 384-399; F. L. Thorp-Greenwood, R. G. Balasingham and M. P. Coogan, *J Organomet Chem*, 2012, **714**; V. Fernandez-Moreira, F. L. Thorp-Greenwood and M. P. Coogan, *Chem Commun (Camb)*, 2010, **46**, 186-202; K. K. Lo, *Accounts of chemical research*, 2015, DOI: 10.1021/acs.accounts.5b00211.
2. Y. You and W. Nam, *Chemical Society reviews*, 2012, **41**, 7061-7084.
3. S. Tobita and T. Yoshihara, *Current opinion in chemical biology*, 2016, **33**, 39-45.
4. K. K. Lo, K. Y. Zhang, S. K. Leung and M. C. Tang, *Angew Chem Int Ed Engl*, 2008, **47**, 2213-2216; K. Y. Zhang, H. W. Liu, M. C. Tang, A. W. Choi, N. Zhu, X. G. Wei, K. C. Lau and K. K. Lo, *Inorganic chemistry*, 2015, **54**, 6582-6593; S. Kumar, Y. Hisamatsu, Y. Tamaki, O. Ishitani and S. Aoki, *Inorganic chemistry*, 2016, **55**, 3829-3843.
5. Y. You, Y. Han, Y. M. Lee, S. Y. Park, W. Nam and S. J. Lippard, *Journal of the American Chemical Society*, 2011, **133**, 11488-11491.
6. S. Ladouceur and E. Zysman-Colman, *Eur J Inorg Chem*, 2013, **2013**, 2985-3007.
7. E. Baggaley, J. A. Weinstein and J. A. G. Williams, *Coordin Chem Rev*, 2012, **256**, 1762-1785; K. K.-W. Lo and K. Y. Zhang, *RSC Advances*, 2012, **2**, 12069.
8. K. Lo, K. Tsang, K. Sze, C. Chung, T. Lee, K. Zhang, W. Hui, C. Li, J. Lau and D. Ng, *Coordin Chem Rev*, 2007, **251**, 2292-2310; K. Y. Zhang, S. P. Li, N. Zhu, I. W. Or, M. S. Cheung, Y. W. Lam and K. K. Lo, *Inorganic chemistry*, 2010, **49**, 2530-2540; K. K. W. Lo, S. P. Y. Li and K. Y. Zhang, *New J Chem*, 2011, **35**, 265-287; S. P. Li, T. S. Tang, K. S. Yiu and K. K. Lo, *Chemistry*, 2012, **18**, 13342-13354; K. K. Lo, A. W. Choi and W. H. Law, *Dalton Trans*, 2012, **41**, 6021-6047; L. Murphy, A. Congreve, L. O. Palsson and J. A. Williams, *Chem Commun (Camb)*, 2010, **46**, 8743-8745; Z. Zhou, D. Li, H. Yang, Y. Zhu and S. Yang, *Dalton Trans*, 2011, **40**, 11941-11944; Y. You, S. Cho and W. Nam, *Inorganic chemistry*,

2014, **53**, 1804-1815; C. Li, M. Yu, Y. Sun, Y. Wu, C. Huang and F. Li, *Journal of the American Chemical Society*, 2011, **133**, 11231-11239; P. K. Lee, H. W. Liu, S. M. Yiu, M. W. Louie and K. K. Lo, *Dalton Trans*, 2011, **40**, 2180-2189; C. Jin, J. Liu, Y. Chen, G. Li, R. Guan, P. Zhang, L. Ji and H. Chao, *Dalton Trans*, 2015, **44**, 7538-7547; S. Moromizato, Y. Hisamatsu, T. Suzuki, Y. Matsuo, R. Abe and S. Aoki, *Inorganic chemistry*, 2012, **51**, 12697-12706; K. Y. Zhang, H. W. Liu, T. T. Fong, X. G. Chen and K. K. Lo, *Inorganic chemistry*, 2010, **49**, 5432-5443.

9. P. Steunenberg, A. Ruggi, N. S. van den Berg, T. Buckle, J. Kuil, F. W. van Leeuwen and A. H. Velders, *Inorganic chemistry*, 2012, **51**, 2105-2114.
10. J. Kuil, P. Steunenberg, P. T. K. Chin, J. Oldenburg, K. Jalink, A. H. Velders and F. W. B. van Leeuwen, *Chembiochem*, 2011, **12**, 1896-1902; C. L. Ho, K. L. Wong, H. K. Kong, Y. M. Ho, C. T. Chan, W. M. Kwok, K. S. Leung, H. L. Tam, M. H. Lam, X. F. Ren, A. M. Ren, J. K. Feng and W. Y. Wong, *Chem Commun (Camb)*, 2012, **48**, 2525-2527; Y. Fan, J. Zhao, Q. Yan, P. R. Chen and D. Zhao, *ACS applied materials & interfaces*, 2014, **6**, 3122-3131.
11. S. Aoki, Y. Matsuo, S. Ogura, H. Ohwada, Y. Hisamatsu, S. Moromizato, M. Shiro and M. Kitamura, *Inorganic chemistry*, 2011, **50**, 806-818; Y. Hisamatsu and S. Aoki, *Eur J Inorg Chem*, 2011, **2011**, 5360-5369; H. Ohmura, H. Yasukawa, T. Minami, Y. Sugi, T. Oba, T. Nagata, S. Kyogoku, H. Ohshima, H. Aoki and T. Imaizumi, *Hypertension research : official journal of the Japanese Society of Hypertension*, 2012, **35**, 1063-1068; Y. Hisamatsu, A. Shibuya, N. Suzuki, T. Suzuki, R. Abe and S. Aoki, *Bioconjug Chem*, 2015, **26**, 857-879; A. Kando, Y. Hisamatsu, H. Ohwada, T. Itoh, S. Moromizato, M. Kohno and S. Aoki, *Inorganic chemistry*, 2015, **54**, 5342-5357.
12. S. Lin, W. Gao, Z. Tian, C. Yang, L. Lu, J.-L. Mergny, C.-H. Leung and D.-L. Ma, *Chem. Sci.*, 2015, **6**, 4284-4290; L. Lu, D. Shiu-Hin Chan, D. W. J. Kwong, H.-Z. He, C.-H. Leung and D.-L. Ma, *Chem. Sci.*, 2014, **5**, 4561-4568; K.-H. Leung, H.-Z. He, B. He, H.-J. Zhong, S. Lin, Y.-T. Wang, D.-L. Ma and C.-H. Leung, *Chem. Sci.*, 2015, **6**, 2166-2171; M. Wang, Z. Mao, T.-S. Kang, C.-Y. Wong, J.-L. Mergny, C.-H. Leung and D.-L. Ma, *Chem. Sci.*, 2016, **7**, 2516-2523.
13. A. Beeby, S. Bettington, I. D. W. Samuel and Z. Wang, *J Mater Chem*, 2003, **13**, 80-83; X. Y. Wang, R. N. Prabhu, R. H. Schmehl and M. Weck, *Macromolecules*, 2006, **39**, 3140-3146.
14. J. Lalevee, M. Peter, F. Dumur, D. Gigmes, N. Blanchard, M. A. Tehfe, F. Morlet-Savary and J. P. Fouassier, *Chemistry*, 2011, **17**, 15027-15031.
15. Bruker, Saint 8.34 software, Madison Wi, USA , 2013.
16. G. M. Sheldrick, *Acta Crystallogr C Struct Chem*, 2015, **71**, 3-8; G. M. Sheldrick, *Acta Crystallogr A Found Adv*, 2015, **71**, 3-8.
17. L. J. B. O. V. Dolomanov, R. J. Gildea, J. A. K. Howeard, H. Puschmann, *Journal of Applied Crystallography*, 2009, **42**, 339-341.
18. G. W. T. M. J. Frisch, H. B. Schlegel, G. E. Scuseria, M. A. Robb, J. R. Cheeseman, G. Scalmani, V. Barone, B. Mennucci, G. A. Petersson, H. Nakatsuji, M. Caricato, X. Li, H. P. Hratchian, A. F. Izmaylov, J. Bloino, G. Zheng, J. L. Sonnenberg, M. Hada, M. Ehara, K. Toyota, R. Fukuda, J. Hasegawa, M. Ishida, T. Nakajima, Y. Honda, O. Kitao, H. Nakai, T. Vreven, J. A. Montgomery, Jr., J. E. Peralta, F. Ogliaro, M. Bearpark, J. J. Heyd, E. Brothers, K. N. Kudin, V. N. Staroverov, T. Keith, R. Kobayashi, J. Normand, K. Raghavachari, A. Rendell, J. C. Burant, S. S. Iyengar, J. Tomasi, M. Cossi, N. Rega, J. M. Millam, M. Klene, J. E. Knox, J. B. Cross, V. Bakken, C. Adamo, J. Jaramillo, R. Gomperts, R. E. Stratmann, O. Yazyev, A. J. Austin, R. Cammi, C. Pomelli, J. W. Ochterski, R. L. Martin, K. Morokuma, V. G. Zakrzewski, G. A. Voth, P. Salvador, J. J. Dannenberg, S. Dapprich, A. D. Daniels, O. Farkas, J. B. Foresman, J. V. Ortiz, J. Cioslowski, and D. J. Fox, *Gaussian 09*, Gaussian, Ing., Wallingford, CT, 2009.
19. A. R. Allouche, *Journal of Computational Chemistry*, 2011, **32**, 174-182.
20. R. Pal, *Faraday Discuss*, 2015, **177**, 507-515.
21. R. Pal and A. Beeby, *Methods and Applications in Fluorescence*, 2014, **2**, 037001.

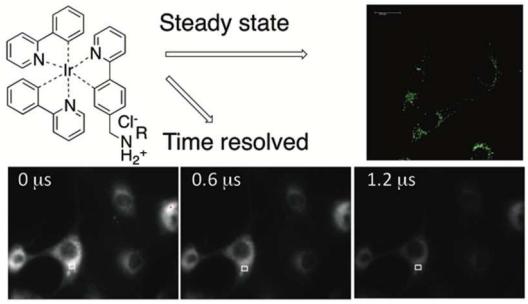

Novel tris-cyclometalated luminescent iridium complexes capable of staining cells and showing *in-cellulo* lifetimes in the micro second regime are reported.